An Experimental Study of Small-Scale Variability of Raindrop Size Distribution

ALI TOKAY

Joint Center for Earth Systems Technology, University of Maryland Baltimore County, Baltimore, and NASA Goddard Space Flight Center, Greenbelt, Maryland

PAUL G. BASHOR

Computer Sciences Corporation, and NASA Wallops Flight Facility, Wallops Island, Virginia

(Manuscript received 29 April 2009, in final form 20 May 2010)

ABSTRACT

An experimental study of small-scale variability of raindrop size distributions (DSDs) has been carried out at Wallops Island, Virginia. Three Joss–Waldvogel disdrometers were operated at a distance of 0.65, 1.05, and 1.70 km in a nearly straight line. The main purpose of the study was to examine the variability of DSDs and its integral parameters of liquid water content, rainfall, and reflectivity within a 2-km array: a typical size of Cartesian radar pixel. The composite DSD of rain events showed very good agreement among the disdrometers except where there were noticeable differences in midsize and large drops in a few events. For consideration of partial beam filling where the radar pixel was not completely covered by rain, a single disdrometer reported just over 10% more rainy minutes than the rainy minutes when all three disdrometers reported rainfall. Similarly two out of three disdrometers reported 5% more rainy minutes than when all three were reporting rainfall. These percentages were based on a 1-min average, and were less for longer averaging periods. Considering only the minutes when all three disdrometers were reporting rainfall, just over one quarter of the observations showed an increase in the difference in rainfall with distance. This finding was based on a 15-min average and was even less for shorter averaging periods. The probability and cumulative distributions of a gamma-fitted DSD and integral rain parameters between the three disdrometers had a very good agreement and no major variability. This was mainly due to the high percentage of light stratiform rain and to the number of storms that traveled along the track of the disdrometers. At a fixed time step, however, both DSDs and integral rain parameters showed substantial variability. The standard deviation (SD) of rain rate was near 3 mm h^{-1}, while the SD of reflectivity exceeded 3 dBZ at the longest separation distance. These standard deviations were at 6-min average and were higher at shorter averaging periods. The correlations decreased with increasing separation distance. For rain rate, the correlations were higher than previous gauge-based studies. This was attributed to the differences in data processing and the difference in rainfall characteristics in different climate regions. It was also considered that the gauge sampling errors could be a factor. In this regard, gauge measurements were simulated employing existing disdrometer dataset. While a difference was noticed in cumulative distribution of rain occurrence between the simulated gauge and disdrometer observations, the correlations in simulated gauge measurements did not differ from the disdrometer measurements.

1. Introduction

The small-scale variability of raindrop size distribution (DSDs) has been recognized through comparative studies of rainfall. Rainfall is an integral parameter of DSDs and the comparative studies have been mainly conducted through rain gauge measurements (e.g., Habib and Krajewski 2002; Gebremichael and Krajewski 2004; Ciach and Krajewski 2006; Villarini et al. 2008). Assuming that the rain gauges are well calibrated, the number and distribution of the gauges within the study area and the experiment period play an important role in determining the small-scale variability of rainfall. Dense gauge networks are mostly in place to validate radar rainfall estimation through a field campaign or provide the database for the hydrological model. Study area and gauge distance vary substantially from one study to the next and therefore small-scale variability is a loose term

Corresponding author address: Ali Tokay, NASA Goddard Space Flight Center, Code 613.1, Greenbelt, MD 20771.
E-mail: tokay@radar.gsfc.nasa.gov

DOI: 10.1175/2010JAMC2269.1

© 2010 American Meteorological Society

and needs to be defined for each study. Krajewski et al. (2003), for example, examined the small-scale variability in five different gauge networks where the maximum gauge separation distance was between 1 and 8 km. In this study, the maximum separation distance is 1.7 km.

One of the main objectives of the small-scale studies is to investigate the intrapixel variability of precipitation products. The ground-based radar rainfall products, for instance, are mostly constructed on 1 km × 1 km or 2 km × 2 km arrays (e.g., Datta et al. 2003). Since the rainfall is a derived product and the reflectivity is a direct measurement, there is an interest to investigate the spatial variability of both variables. In that regard, disdrometers provide the most relevant data source to study spatial variability of rainfall and reflectivity. Relative to the rain gauge network, the construction of a disdrometer network is costly and has additional logistic challenges. Therefore, to our knowledge, there were only a few studies that used a disdrometer network in the literature (Miriovsky et al. 2004; Lee et al. 2009). However, it is expected that recent developments in optical disdrometers such as the one developed by Löffler-Mang and Joss (2000) provide necessary resources in constructing affordable dense disdrometer networks.

Outside the atmospheric sciences community, the small-scale variability of raindrop size distribution and its integral parameters are of interest to hydrologists, engineers, and agricultural and soil scientists. Hydrologists consider the sensitivity of hydrological models to the spatial variability of rainfall and its influence on flood prediction (Arnaud et al. 2002). Engineers try to formulate the attenuation by precipitation (Asen and Gibbins 2002). Soil scientists use a relation between the kinetic energy of raindrops and rain intensity to determine soil erosivity (van Dijk et al. 2002).

The nonuniform beam filling within the footprint of an airborne or spaceborne radar, or within the pixel of a ground-based radar, significantly contributes to the error in radar rainfall estimation. Kozu and Iguchi (1999) presented a method of nonuniform beam filling correction for the path-integrated attenuation derived from spaceborne radar measurements employing Tropical Ocean and Global Atmosphere Coupled Ocean–Atmosphere Response Experiment (TOGA COARE) radar-derived rainfall product at 1 km × 1 km resolution. The key to the correction in their method was the estimation of the small-scale rainfall variability within the footprint. Zhang et al. (2004) revisited the nonuniform beam filling correction of Kozu and Iguchi (1999) by employing X-band radar at 125-m-range resolution for a study located near Beijing, China. They reported that the nonuniform beam filling resulted in an underestimation in the path-integrated attenuation up to 50% for a spaceborne radar footprint of 0.5 km.

For the same reflectivity gradient, the nonuniform beam filling error in ground-based radars is a function of the pixel size of the radar that increases with distance from the radar site. The pixel size at a given distance is a function of the beamwidth and range gate spacing of the radar. While the variability of rainfall within the pixel domain is related to the nonuniform beam filling, the pixel may be partially covered by a rain-free region as well. High temporal resolution disdrometer observations can provide an insight for rain versus no-rain signal with the radar pixel.

As noted above, the rain gauge networks have been widely used to study the variability of rainfall within a ground-based radar pixel. Habib and Krajewski (2002) and Gebremichael and Krajewski (2004), for instance, used the gauge networks in central Florida and the Amazon basin of Brazil, respectively, where the networks were designed to provide a validation dataset for the radar rainfall estimation. Both studies showed a decrease in the correlation coefficient of rain rate with increasing gauge separation distance where the tipping-bucket gauge observations were averaged at least 5 min to avoid severe sampling errors (Habib et al. 2001b). Interestingly, the most rapid decrease in correlation occurred within the first 2-km separation distance in both studies. More recently, Ciach and Krajewski (2006) examined the dependence of small-scale variability of rainfall on time averaging, interstorm variability, and rainfall intensity. Their study was based on 25 gauge stations at a 3 km × 3 km array in central Oklahoma. Villarini et al. (2008), on the other hand, used 50 gauges in a 135 km^2 area in southwestern England to evaluate the temporal and spatial sampling uncertainties of remote sensing rainfall products. The correlations also decreased with increasing gauge separation distances, but the degree of decrease was much less for longer integration periods in these two studies.

As a pioneer study, Miriovsky et al. (2004) employed a set of five different types of disdrometers to study the small-scale variability of reflectivity. The disdrometers were deployed in a 1 km^2 area and significant variability of reflectivity was reported within the observational area. The authors did not make the quantitative statement on small-scale variability of rainfall because of instrument uncertainties and limited sample of rainfall (20 h). Lee et al. (2009) studied the spatial variability of DSDs and the bulk parameters of rainfall and reflectivity through four Precipitation Occurrence Sensor System (POSS) disdrometers. The disdrometers were separated from 1.3 to 32.6 km and they found significant variations in event-averaged DSDs and in rainfall and

reflectivity in stratiform events. The event-average-based reflectivity gradient, for instance, reached about 1.2 dB at 1.3-km distance.

In this study, we employed three impact-type Joss–Waldvogel (JW) disdrometers to study the small-scale variability of DSDs through gamma-fitted parameters and the integral products of liquid water content, rainfall, and reflectivity. Our main goal was to evaluate the spatial variability of DSDs within a ground-based radar pixel. It should be noted that there is no consensus in terminology for "small scale" variability of raindrop size distribution or its integral product in the literature. In their introductory statements, Gebremichael and Krajewski (2004) described the small-scale as under 20 km for rainfall measurements while Berne et al. (2004) stated on the order of 10 km for the hydrological applications. We defined small-scale as the resolution of a rain sensing instrument under which the knowledge of spatial variability requires measurements by other instruments.

Considering ground-based radars, the disdrometer network is the sole choice to study spatial variability of radar reflectivity within pixel space. Since the radar measurements are instantaneous over the pixel space, the highest temporal resolution of disdrometer measurements is required to study the small-scale variability. In recent years, polarimetric radar measurements have been used to derive the DSD (e.g., Bringi et al. 2003; Zhang et al. 2001). These studies often employ a parametric form of gamma distribution parameters. Our study investigates the changes in gamma size distribution parameters within a single radar pixel.

The sampling errors are one of main shortcomings of the *point* disdrometer measurements and time averaging intends to reduce the sampling variability. Amitai et al. (2006) presented the role of time averaging in rain gauge measurements during construction of reflectivity versus rainfall table, while Steiner and Smith (2004) showed approximately 3-dB reduction in reflectivity when the DSD is averaged over 5 min. On should keep in mind that the time averaging reduces the physical variability. Here, we considered five different disdrometer time average periods, ranging from 1 to 15 min.

We organized this paper as follows: Following a brief description of Joss–Waldvogel disdrometer and data processing in section 2, the experiment site and setup is described in section 3. The characteristics of rain events are presented in section 4, while the differences in event-based average raindrop spectra and derived rain parameters are discussed in the following section. Section 6 focuses on the disdrometer sampling issues, and probability of rainfall is presented in section 7. The spatial variability of DSDs through gamma-fitted parameters as well as integral rain parameters at various time-averaging periods are discussed in section 8, and spatial variability of simulated gauge rainfall measurements are presented in section 9. We offer concluding remarks in the last section of the manuscript.

2. Joss–Waldvogel disdrometer

The JW disdrometer is an impact type of disdrometer consisting of a sensor head and signal processing electronics. The surface cross section is 50 cm^2 and measures drops from 0.3- to about 5.3-mm diameter within $\pm 5\%$ accuracy. The JW disdrometer has been commercially available for over 40 years, and there have been no major changes in its measuring principles (Joss and Waldvogel 1967). The shortcomings of the JW disdrometer have been well documented in literature (e.g., Tokay et al. 2005). In brief, it underestimates the small drops in the presence of background noise and electrical interference. It also underestimates the small drops in heavy rain (>10 mm h^{-1}), which is known as disdrometer's dead time. The disdrometer cannot distinguish very large drops (>5 mm in diameter). These raindrops are recorded in the disdrometer's last size bin of which its center diameter is around 5.1 mm. Like other types of disdrometers, it requires power and a shelter for its processor, which is linked to a personal computer. This limits site location choices when designing a study for the small-scale variability of DSDs. It is possible, however, to utilize a cable as long as 100 m between the sensor and processor, to provide some flexibility for the site selection.

Considering the data processing, a registering raindrop is recorded on one of the 127 channels of the JW disdrometer and the channel counts are stored in 10-s intervals. The measurements are then averaged to 1 min and the drops are grouped into 20 standard size bins of the JW disdrometer. The midsize diameter of each bin is calculated based on a vendor-supplied calibration table that is unique for each disdrometer. The bulk descriptors of rainfall—namely, total number of drops, concentration, liquid water content, rain rate, and reflectivity—are calculated for each minute of spectra, without dead time correction. Raindrop spectra containing fewer than 10 drops or with a rain rate less than 0.1 mm h^{-1} is disregarded as noise. A rain event is defined based on 1 h or longer rain-free period between the two consecutive rainy minutes.

3. Experiment site and setup

As part of the National Aeronautics and Space Administration (NASA) Tropical Rainfall Measuring Mission (TRMM) Ground Validation program (Wolff et al.

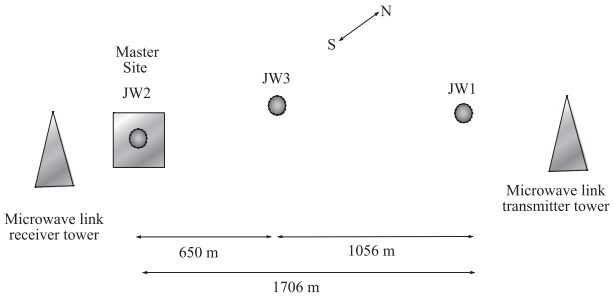

FIG. 1. The disdrometer network between the transmitter and receiver end of microwave link towers.

FIG. 2. A picture of the sensor of the JW disdrometer at NASA Wallops Flight Facility, Wallops Island, VA.

2005), a disdrometer and rain gauge test facility has been operating at NASA Wallops Flight Facility at Wallops Island, Virginia, for approximately 10 years (Tokay et al. 2005). Wallops Island (37.84°N, 75.48°W) is located along the mid-Atlantic coast of the United States and receives nearly 100 cm of precipitation annually with less than 3-cm difference between the months that receive maximum and minimum precipitation. It is subject to frontal and convective rainfall as well as remnants of Atlantic Ocean hurricanes.

To evaluate the path-averaged raindrop size distribution retrieved from dual-frequency microwave link measurements, three JW disdrometers were placed between the transmitter and receiver end of the link towers (Fig. 1) in March 2001 and were swapped several times because of unexpected failures and for maintenance in 2002. Here, we used four months of disdrometer measurements between mid-May and mid-September 2003. The disdrometers sit on a thin water-absorbing material placed on cinder blocks as shown in Fig. 2 and were placed in a nearly straight line with distances of 0.65, 1.05, and 1.70 km.

4. Rainfall measurements

A total of 40 rain events with rain accumulation of 1 mm or higher were recorded during the experimental period. The disdrometer at the master site (JW2) recorded 484.81 mm of rainfall, nearly 2.5% and 5.0% more rainfall than the units in the middle (JW3) and the opposite end (JW1), respectively (Fig. 3a). JW3 recorded 8200 rainy minutes, 80 and 132 min more rainfall than JW2 and JW1, respectively. The differences in rainy minutes are due in part to the natural variability of rainfall and in part to data processing. It could well be that one of the disdrometers recorded 9 drops or just less than 0.1 mm h^{-1} rainfall, just under the minimum total number of drops or rain rate threshold to be defined as a rainy minute. The composite spectra were nearly identical with the exception that JW3 recorded less drops at sizes larger >4.0 mm in diameter (Fig. 3b). It is interesting to note that the differences in experiment-long rain accumulations and in composite spectra were much higher in a similar study in Iowa presented by Miriovsky et al. (2004). Aside from differences in characteristics of precipitation in Iowa City, Iowa, and Wallops Island, the difference in sampling size and the use of the same type of disdrometers versus different types likely also contributed to the different results of the two studies.

For the rain event statistics, the percent mean absolute rain total difference is the largest between JW1 and JW2 and the smallest between JW2 and JW3 (Fig. 3c). This coincides with the longest and the shortest separation distance, but only a quarter of the rain events exhibit the largest difference with the maximum separation distance and the smallest difference with the minimum separation distance. Interestingly, the differences were 11.5% or less, which can be also observed between collocated in situ rain measuring instruments (Tokay et al. 2003). If a single disdrometer is used to verify the corresponding radar pixel rain estimate, the natural variability of rainfall within the pixel could lower the agreement between the radar and disdrometer rainfall.

The percent mean absolute rain total difference between jth and kth disdrometers $\langle \Delta \mathrm{RT} \rangle$ is given as

$$\langle \Delta \mathrm{RT}_{j,k} \rangle = \frac{\frac{1}{N}\sum_{i=1}^{N} |\mathrm{RT}_{j,i} - \mathrm{RT}_{k,i}|}{\frac{1}{N}\sum_{i=1}^{N} (\mathrm{RT}_{j,i} + \mathrm{RT}_{k,i})/2}, \qquad (1)$$

where N is the number of rain events.

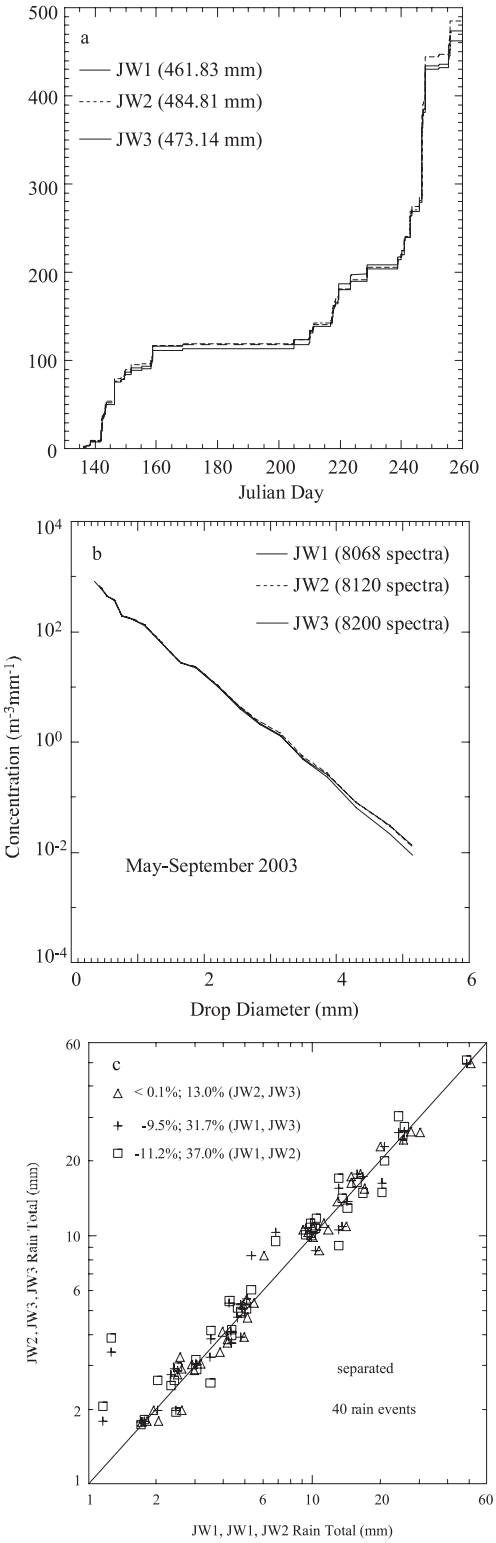

FIG. 3. (a) Accumulative rainfall of three JW disdrometers from 40 rain events from May through September 2003. (b) Composite drop size distributions from three JW disdrometers. The number of 1-min spectra in each composite is shown in parentheses. (c) Scatter diagram of event rain totals between a pair of disdrometers when they were separated. The mean event rain totals difference and its standard deviation are also given.

5. Composite raindrop spectra

To study the small-scale variability of DSDs on an event basis, we selected nine rain events where the event rain totals were at least 14 mm or higher. These nine rain events exhibited diversity in terms of duration and intensity of rainfall. These events were also diverse in terms of precipitation type. Table 1 presents the date, start and end time, and mean and maximum rain intensity of the events based on JW3. The event rainy minutes when all three units reported rainfall, range of event rain total, and percent occurrences of rain rates <5 mm h^{-1} and >10 mm h^{-1} are also given in Table 1. The occurrence of rain rate <5 mm h^{-1} mainly represents stratiform in the presence of light to moderate rainfall. Indeed, the radar loops from Weather Surveillance Radar-1988 Doppler (WSR-88D) in Wakefield, Virginia (KAKQ), showed widespread echo structure in events 1 and 3 where a very high percentage of light to moderate rainfall was observed at the disdrometer site. The lines of high-reflectivity (larger than 40 dB) echoes were present in WSR-88D loops for the rest of the events. These lines of high echoes were either embedded within the low echo (less than 30 dB) region (events 2, 4, 5, and 8) or acted as a leading edge of the system (events 6, 7, and 9). The partitioning between low and high echo regions from one event to another varied substantially at the disdrometer site depending on orientation and size of the precipitation bands. The percent of heavy rainfall is therefore quite different from one event to another. The north-to-south elongated precipitation in events 2 and 4 and small precipitation cell in event 8 resulted in shorter durations among 9 major rain events. The disdrometer site experiences long duration of high reflectivity in event 8; while a low-reflectivity region dominated the disdrometer site in event 6. The high and low percentages of heavy rain in these events reflected the echo structures. Considering all nine events, the disdrometer site experienced 77% of light to moderate and 15% of heavy rain. The rain rate interval between 5 and 10 mm h^{-1} is considered moderate to heavy rain and was excluded from event percent rain occurrence as shown in the last column of Table 1. Mainly, it is hard to relate this rain rate interval to convective or stratiform rainfall.

The comparison of the composite raindrop spectra among the three disdrometers in nine rain events provided more in-depth information regarding the small-scale variability of DSDs (Fig. 4). Here, we examined the

TABLE 1. Rainfall characteristics of the nine major rain events.

Event no.	Date	Start time (UTC)	End time (UTC)	Rainy minutes	Mean and max rain rate (mm h^{-1})	Rain total (mm)	% occurrence (rain rate < 5 mm h^{-1}, rain rate > 10 m h^{-1})
1	21–22 May	2207	1300	869	1.8, 6.8	25.75–27.51	97, 0
2	26 May	0912	1116	85	17.1, 129.8	24.26–25.45	56, 38
3	7 Jun	1044	0217	792	1.7, 47.2	20.06–22.86	92, 2
4	5 Aug	1339	1621	113	9.4, 120.2	15.78–17.74	85, 12
5	7 Aug	1225	1705	259	4.0, 44.8	14.90–17.30	76, 9
6	29 Aug	0523	0641	79	12.4, 101.6	14.94–20.39	67, 32
7	30–31 Aug	2354	0518	322	4.8, 67.4	24.30–30.29	80, 10
8	3 Sep	1706	2235	313	16.6, 84.5	84.03–91.44	31, 53
9	4 Sep	1949	0214	214	13.8, 112.2	48.03–50.99	58, 35

differences in fitted normalized gamma distribution and integral rainfall parameters in terms of small (diameters <1 mm), medium-size (diameters 1–3 mm), and large drops (diameters >3 mm). The normalized gamma distribution is often employed to estimate the DSD parameters from dual-polarized (Bringi et al. 2003) or dual-wavelength (Meneghini and Liao 2007) radar measurements. The normalization of gamma distribution was done with respect to the total concentration N_T and liquid water content W. The normalized intercept parameters with respect to total concentration N_T^* and liquid water content N_W are expressed as

$$N_T^* = \frac{N_T}{D_{\text{mass}}} \quad \text{and} \tag{2}$$

$$N_w = \frac{256}{\pi\rho_w}\frac{10^3 W}{D_{\text{mass}}^4}, \tag{3}$$

where D_{mass} is the mean mass diameter and ρ_w is the density of water. The mean mass diameter is directly calculated from observed DSD and is related to the slope Λ and shape parameters m of the gamma distribution as

$$D_{\text{mass}} = \frac{4+m}{\Lambda}. \tag{4}$$

The normalized intercept parameters can then be calculated from observed spectra as well. The corresponding normalized gamma-fitted distributions are expressed as

$$N(D) = N_T^* f_1(m)\left(\frac{D}{D_{\text{mass}}}\right)^m \exp\left[-(4+m)\frac{D}{D_{\text{mass}}}\right] \quad \text{and} \tag{5}$$

$$N(D) = N_w f_2(m)\left(\frac{D}{D_{\text{mass}}}\right)^m \exp\left[-(4+m)\frac{D}{D_{\text{mass}}}\right], \tag{6}$$

where $f_1(m)$ and $f_2(m)$ are given as

$$f_1(m) = \frac{(4+m)^{m+1}}{\Gamma(m+1)} \quad \text{and} \tag{7}$$

$$f_2(m) = \frac{6}{256}\frac{(4+m)^{m+4}}{\Gamma(m+4)}. \tag{8}$$

To extract the shape parameter, we minimize the error in rain rates that are calculated from observed spectra and from fitted gamma distribution in Eqs. (5) and (6). The parameters of fitted gamma distribution and integral rainfall parameters for nine major events are listed in Tables 2 and 3, respectively.

The agreement in small drop regime was good in all cases and the composite spectra showed no drop off in small size, a typical shortcoming of the JW disdrometer. This hints that the small drops are adequately measured and concentration and related normalized intercept parameters are accurate. Among all cases, the agreements in midsize and large drops are also good, with a few exceptions. The number of midsize and large drops was noticeably higher in JW1 in event 6, while JW1 and JW3 had higher concentrations of large drops in events 5 and 7, respectively. In these three events, the mean mass diameter showed the highest variation, 0.11-mm difference (Table 2). The shape parameters were consistent in all cases where the differences were less than one, while normalized intercept parameters N_T^* and N_w experienced differences less than 50 and 300 mm^{-1} m^{-3}, respectively.

Considering integral rainfall parameters, the small and/or midsize drops are the main contributors to the total concentration, liquid water content, and rain rate, while midsize and/or large raindrops are the main contributors to reflectively. This is because liquid water content and rain rate are proportional to the third and third-to-fourth moment of drop diameter, respectively, while the reflectivity is proportional to the sixth moment of the drop diameter. The largest differences in liquid water content and rain rate were 0.166 g m^{-3} and 4.3 mm h^{-1}, respectively, and occurred in event 6

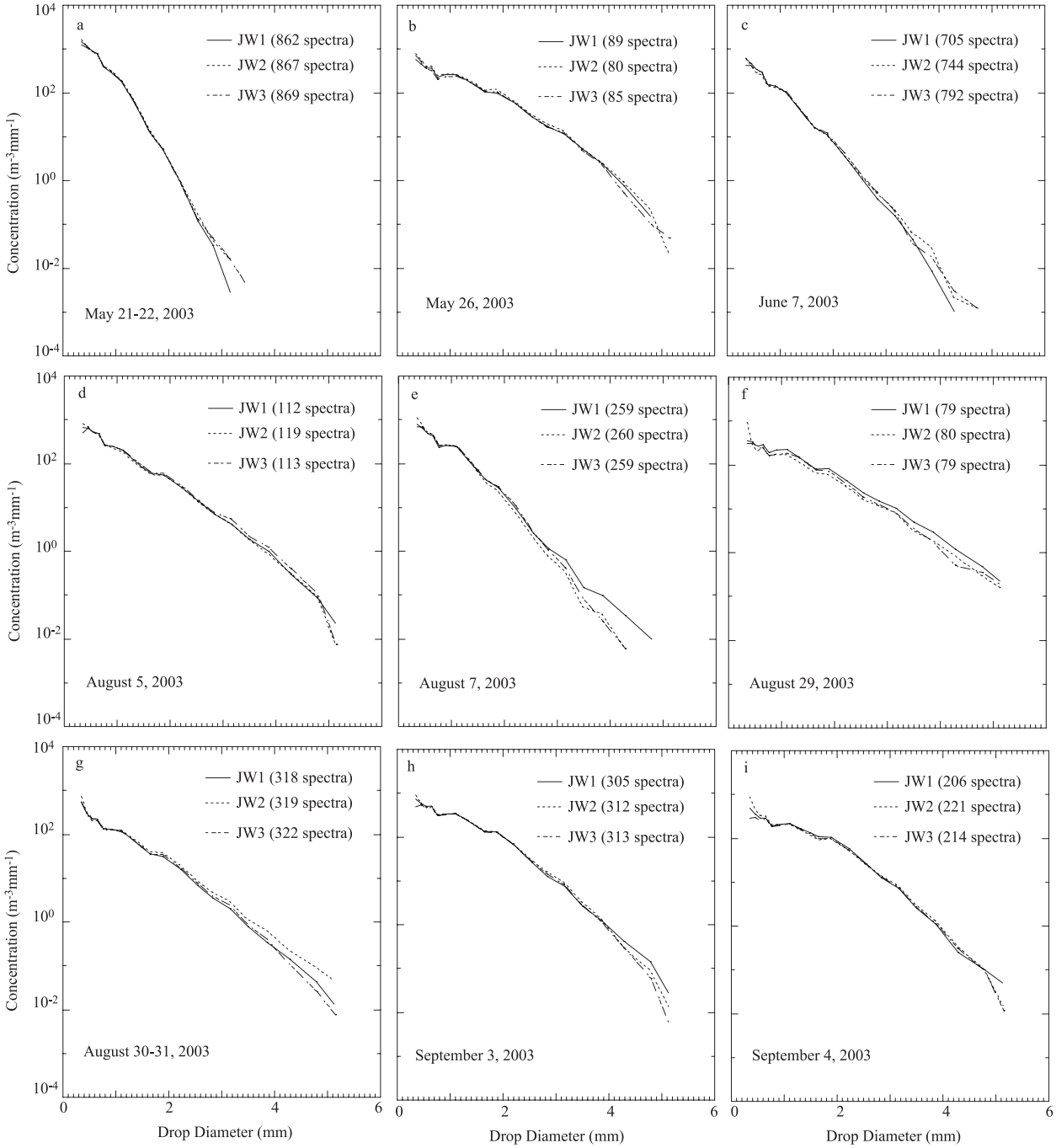

FIG. 4. Composite raindrop spectra from nine major rain events. The rainfall characteristics of each event can be found in Table 1.

(Table 3). This corresponded to 30% differences in both integral parameters. The differences in reflectivity exceeded 1 dB for events 5, 6, and 7.

6. Sampling issues

Disdrometer measurements are often employed to derive an empirical relation between the radar reflectivity Z and rain rate R for a precipitation event, storm type, or a climate region. The robustness of such relations relies on sampling and the sample size (Jameson and Kostinski 2001). The sampling is related to the data processing where the three major factors are the minimum number of drops, rain rate threshold of each sample, and time averaging. Steiner and Smith (2000, 2004) and Tokay et al. (2005) examined the influence of each factor to the

TABLE 2. Normalized gamma size distribution parameters that were fitted to the composite raindrop spectra of each disdrometer for nine major rain events. The parameters include normalized intercept parameter with respect to the total concentration N_T^* and with respect to the liquid water content N_w, mean mass diameter D_{mass}, and shape parameter when N_T^* and N_w are employed.

Event no.	N_T^*, N_w (JW1) ($\mathrm{mm^{-1}\ m^{-3}}$)	N_T^*, N_w (JW2) ($\mathrm{mm^{-1}\ m^{-3}}$)	N_T^*, N_w (JW3) ($\mathrm{mm^{-1}\ m^{-3}}$)	D_{mass} (JW1) (mm)	D_{mass} (JW2) (mm)	D_{mass} (JW3) (mm)	Shape parameter (JW1)	Shape parameter (JW2)	Shape parameter (JW3)
1	577, 8589	593, 8659	537, 8248	1.04	1.06	1.06	3.0, 2.2	2.9, 2.2	3.1, 2.3
2	201, 2155	228, 2385	204, 2211	2.27	2.28	2.26	1.7, 3.4	1.6, 3.4	1.7, 3.7
3	189, 2012	169, 1721	168, 1858	1.39	1.44	1.43	1.6, 1.1	1.5, 1.0	1.8, 1.2
4	212, 1724	212, 1634	204, 1709	2.05	2.07	2.11	1.0, 1.4	0.9, 1.5	1.1, 1.5
5	275, 3169	330, 3896	288, 3620	1.52	1.41	1.48	1.9, 1.5	2.0, 1.9	2.2, 2.2
6	143, 1451	145, 1178	136, 1429	2.43	2.37	2.32	1.5, 2.5	1.0, 2.2	1.6, 2.5
7	123, 1077	130, 1034	119, 1069	1.99	2.10	2.01	1.2, 1.7	1.0, 1.6	1.2, 2.2
8	284, 3337	288, 3338	261, 3299	2.05	2.08	2.06	2.0, 3.1	2.0, 3.5	2.3, 3.6
9	181, 2326	200, 2112	161, 2151	2.14	2.18	2.17	2.3, 4.4	1.7, 3.9	2.5, 4.5

R–Z relationship through long-term disdrometer measurements. Since large drops occur in fewer amounts in a raindrop spectrum and because they have a pronounced effect on reflectivity, sampling is more of an issue for the reflectivity than the rain rate (Smith et al. 1993). The higher thresholds for the number of drops and rain rate omit light rain and decrease sample size. Similarly, time averaging decreases the sample size and may distort the nature of precipitation. Unfortunately, there is no consensus in regard to the standard disdrometer data processing in the literature. Hagen and Yuter (2003), for example, tried to reduce the sampling errors without distorting the nature of precipitation, applying 10-min averaging to the 1-min disdrometer measurements where the minimum number of drops was 20 and rain rate threshold was 2 mm $\mathrm{h^{-1}}$. It is also true that different disdrometer types have different sampling volumes. The POSS, for instance, has 3 times more sample volume than the JW disdrometer (Lee et al. 2009), so the criterion for the thresholds should be different for different disdrometers.

In this study, we considered time averaging in calculating the statistical parameters that will help to determine the small-scale variability of DSDs and their integral rainfall parameters in a quantitative manner. We adopted the time averaging where there is no requirement of rainfall in all minutes that are included in the averaging. This was unconditional averaging and the sample size for 1-, 3-, 6-, 10-, and 15-min averaging are shown in Table 4. To show the importance of differences in the averaging method, we presented the sample size of 3-, 6-, 10-, and 15-min average size distributions where all the minutes reported rainfall in Table 4 as well. This was conditional averaging. The difference in sample size between the two different averaging methods increased from 16% for 3-min averaging to 56% for 15-min averaging. Adopting the first method, we had more than 500 samples for the analysis presented below.

7. Rain versus no-rain probability

As stated in the introduction, nonuniform beam filling due to partially precipitating radar pixel or satellite footprint is a key source of error in retrieving rainfall from remote sensing instruments. In this study, we examined the differences in rainy minutes between one or

TABLE 3. Liquid water content *W*, rain rate *R*, and reflectivity *Z* calculated from composite raindrop spectra of each disdrometer for nine major rain events.

Event no.	*W* (JW1) ($\mathrm{g\ m^{-3}}$)	*W* (JW2) ($\mathrm{g\ m^{-3}}$)	*W* (JW3) ($\mathrm{g\ m^{-3}}$)	*R* (JW1) ($\mathrm{mm\ h^{-1}}$)	*R* (JW2) ($\mathrm{mm\ h^{-1}}$)	*R* (JW3) ($\mathrm{mm\ h^{-1}}$)	*Z* (JW1) (dB*Z*)	*Z* (JW2) (dB*Z*)	*Z* (JW3) (dB*Z*)
1	0.125	0.132	0.126	1.8	1.9	1.8	26.1	26.5	26.3
2	0.708	0.790	0.710	17.1	19.1	17.1	43.6	44.1	43.5
3	0.091	0.090	0.096	1.6	1.6	1.7	28.8	29.3	29.4
4	0.376	0.365	0.412	8.4	8.2	9.4	40.0	39.9	40.7
5	0.207	0.191	0.215	3.9	3.4	4.0	33.5	32.1	33.1
6	0.624	0.458	0.511	15.5	11.2	12.4	44.2	42.6	42.8
7	0.207	0.249	0.216	4.6	5.7	4.8	36.9	38.5	37.1
8	0.724	0.763	0.724	16.5	17.6	16.6	42.5	42.8	42.4
9	0.604	0.584	0.584	14.2	13.8	13.8	42.1	42.2	42.0

TABLE 4. Number of rainy minutes for five different averaging periods where no condition and condition (only rainy minutes are included) was applied to the averaging process. The percent reduction in sample size is also shown.

Time averaging (min)	Rainy minutes (unconditional)	Rainy minutes (conditional)	Reduction (%)
1	7598	7598	0
3	2711	2264	16.5
6	1433	994	30.6
10	913	522	42.8
15	639	279	56.3

two and all three disdrometers reporting rainfall. We used the terminology ''base'' rainy minutes for the period all three units reported rainfall. The percent difference in rainy minutes for the jth disdrometer, ΔN_j from base rainy minutes is given as

$$\Delta N_j = 100\frac{N_j - N_{j,k,l}}{N_j}, \tag{9}$$

where N_j and $N_{j,k,l}$ represent rainy minutes of jth and of jth, kth, and lth disdrometers together, respectively. Table 5 presents the percent rain minute differences of 1-, 3-, 6-, 10-, and 15-min average disdrometric measurements. The disdrometer in the middle had the highest rain occurrence, having 6.9%–10.6% more rainy minutes than the base rainy minutes. Narrow precipitation bands passing perpendicular to the base line of disdrometers are expected to leave more rain either on the left or right side of the disdrometer network. At the same time, a small percentage of unorganized precipitation bands may pass two ends with a precipitation gap in the middle. In that regard, two end units reported rainfall only 0.5%–1.3% higher than base rainy minutes. During this study, rainfall occurred more at the left side of the network than the right side of the network since JW2 had higher rainy minutes than JW1. The passage of precipitation bands toward the left side of the network resulted in 2.5%–5.7% more rainy minutes in JW2 and JW3 than base rainy minutes, while JW1 and JW3 jointly had 1.5%–2.4% more rain the base rainy minutes.

8. Small-scale variability

Prior to the analysis of the small-scale variability of DSDs and integral rain parameters at various time-averaging periods, we asked a fundamental question: Should one expect an increase in the difference of bulk descriptors of rainfall with distance at spatial scales less than 2 km? Although one may respond to this question with ''yes,'' our analysis showed that this is not always true. Tables 6 and 7 show the percent time of the observations where the difference in rain rate and reflectivity, respectively, increased with distance for 1-, 3-, 6-, 10-, and 15-min averages. About 60%–68% of the observations had greater rain rate difference between the two farthest stations than that between the two closest stations. In contrast, only 22%–26% of observations showed the increase in rain rate difference with distance for all three distances. In terms of reflectivity, about 59%–67% of the observations had greater reflectivity difference between the two farthest stations than that between the two closest stations, while only 20%–27% of observations showed the increase in reflectivity difference with distance for all three distances. Here, both rain rate and reflectivity are calculated based on their linear units of mm h^{-1} and mm^6 m^{-3}, respectively. The presence of a high percentage of light stratiform rain (Fig. 5e) contributed significantly to the cause of not observing increase–decrease in rain parameter in a radial direction in spatial scale of 2 km at all times.

Another step we have taken prior to analysis of the small-scale variability of DSDs and integral rain parameters was to examine the distributions of each parameter. Employing 1-min averages where all three disdrometers reported rainfall, probability, and cumulative distributions of five DSDs and three integral rain parameters showed small variability (Fig. 7). The differences in mean normalized intercept parameters N_T^* and N_W were less than 4% and 3%, respectively. The mean mass diameter had 1% differences between its mean values, and the shape parameters with respect to N_T^* and N_W had 9% and 4% differences in their means, respectively. Considering integral rain parameters, the difference in mean liquid water contents was <5%, while a 10% difference occurred between the mean rain

TABLE 5. Percent rainy minutes for which either one or two disdrometers reported rainfall in excess of all three disdrometers reported.

Time averaging (min)	JW1 > 0 (%)	JW2 > 0 (%)	JW3 > 0 (%)	JW1 > 0 and JW2 > 0 (%)	JW1 > 0 and JW3 > 0 (%)	JW2 > 0 and JW3 > 0 (%)
1	8.13	8.90	10.58	1.31	2.41	5.69
3	4.83	5.72	7.67	0.77	1.95	3.25
6	3.98	4.88	7.12	0.35	1.81	2.79
10	3.40	4.38	6.13	0.77	1.53	2.63
15	3.29	4.23	6.89	0.47	1.88	2.50

TABLE 6. Percent rainy minutes for which the absolute difference in rain rate at distance Dx (x = 2, 3) is greater than that at distance Dy (y = 1, 2); D1, D2, and D3 represent $|\Delta R|$ (0.65 km), $|\Delta R|$ (1.05 km), and $|\Delta R|$ (1.70 km), respectively.

Time averaging (min)	D3 > D1 (%)	D3 > D2 (%)	D2 > D1 (%)	D3 > D1 and D3 > D2 (%)	D3 > D1 and D2 > D1 (%)	D3 > D2 and D2 > D1 (%)
1	60.25	55.34	54.42	42.19	40.04	21.98
3	63.74	56.88	58.02	44.41	44.78	25.45
6	65.04	56.94	58.76	45.71	45.50	26.17
10	65.50	58.82	56.95	46.88	44.03	25.41
15	68.07	57.75	58.68	46.48	47.57	25.98

rates. The mean reflectivities, on the other hand, had 0.34-dBZ difference. It should be noted that all the mean values were calculated from linear values of each parameter except for reflectivity in its logarithmic scale. For plotting purposes (Fig. 5), most of the parameters except for D_{mass} and the shape parameters were plotted in logarithmic scale.

The differences in cumulative distribution of rain and reflectivity between the disdrometers were substantially larger in a similar study by Miriovsky et al. (2004). As stated above, a much larger sample size and the use of the same type of disdrometers played an important role in the agreement between the rainfall and reflectivity cumulative distributions.

The standard deviation of the difference (SD) and Pearson product-moment correlation coefficient were employed between the pairs of disdrometer measurements to determine the small-scale variability of DSDs and integral rain parameters. The SD of rain parameter X between ith and jth disdrometers is the square root of the product of summation of variances of X_i and X_j minus 2 times covariance between X_i and X_j and is given as

$$\mathrm{SD}(X_{i,j}) = [\mathrm{Var}(X_i) + \mathrm{Var}(X_j) - 2\,\mathrm{Cov}(X_i, X_j)]^{1/2}. \tag{10}$$

The SD is expressed with the unit of the X variable. Considering an alternative statistic, there was literally no difference between SD and root-mean-square difference for any X parameter of interest in this study. The fractional standard deviation (FSD), which is the ratio of SD to the mean of the two variables, is also calculated but is not plotted since it has the same trend of SD. The FSD is a normalized quantity and provides additional information on the variability of the parameter.

The Pearson product-moment correlation coefficient has been widely used in small-scale variability of rainfall (e.g., Krajewski et al. 2003). It is a normalized quantity and is neither robust nor resistant (Wilks 1995). Habib et al. (2001a) assessed the significance of the Pearson correlation coefficient of rainfall by investigating its sensitivity to sample size, extreme rain rates, and departures from normal distribution. They recommended an alternative correlation coefficient that requires a log-normally distributed integral parameter. The correlation coefficient from the Pearson method was higher than that from their method.

The SD increases with distance and mostly decreases as the integration period increases (Fig. 6). While 1-min average statistics are more relevant to examine the small-scale variability in a radar pixel space, they are also affected the most from sampling issues. Here, we considered 6-min average statistics as reference and focused on the variability of the statistic at the shortest and longest separation distances. The SD of N_T^*, for instance, varied from 122 mm^{-1} m^{-3} at the shortest to 204 mm^{-1} m^{-3} at the longest separation distance (Fig. 6a) and the corresponding FSD were 0.38 and 0.62. The SD of N_w, on the other hand, had a range from 3684 to 6630 mm^{-1} m^{-3} (Fig. 6b) and the corresponding FSD were 0.53 and 0.94. The mean mass diameter had a SD of 0.10 and 0.18 mm at the shortest and longest distance (Fig. 6c), corresponding to FSD of 0.08 and 0.14. The shape parameters in Eqs. (5) and (6) had a SD from 1.7

TABLE 7. As in Table 6, but where D1, D2, and D3 represent $|\Delta Z|$ (0.65 km), $|\Delta Z|$ (1.05 km), and $|\Delta Z|$ (1.70 km), respectively.

Time averaging (min)	D3 > D1 (%)	D3 > D2 (%)	D2 > D1 (%)	D3 > D1 and D3 > D2 (%)	D3 > D1 and D2 > D1 (%)	D3 > D2 and D2 > D1 (%)
1	59.27	55.05	53.41	41.39	38.35	20.48
3	63.04	56.36	56.07	44.96	42.79	24.71
6	66.78	57.43	58.76	47.24	45.64	26.10
10	64.95	60.35	55.42	47.43	42.93	25.41
15	66.98	59.47	58.53	47.57	46.48	27.07

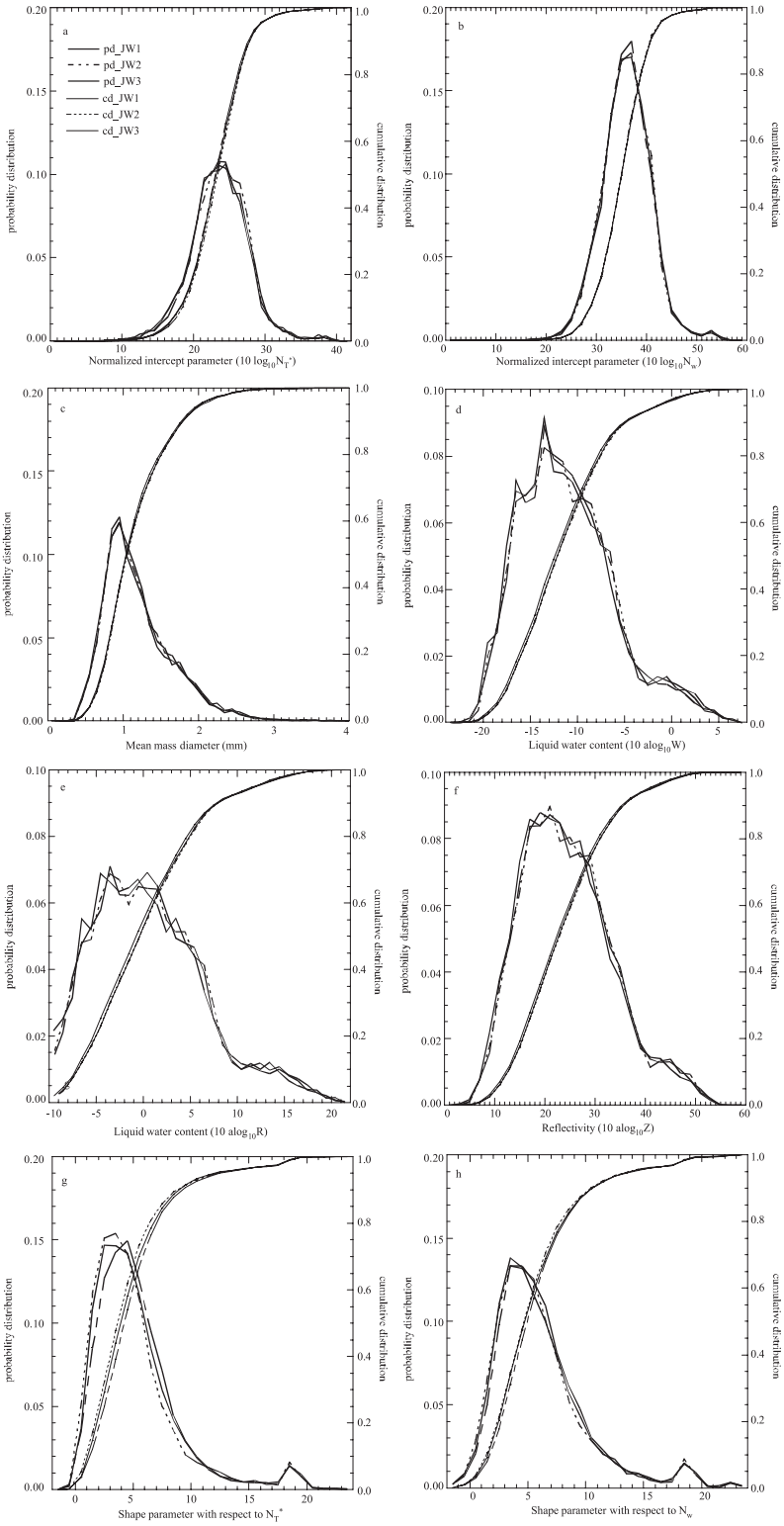

FIG. 5. The probability (light lines) and cumulative (dark lines) distributions of (a) normalized intercept parameter N_T^*, (b) normalized intercept parameter N_w, (c) mean mass diameter, (d) liquid water content, (e) rain rate, (f) reflectivity, (g) shape parameter with respect to N_T^*, and (h) shape parameter with respect to N_w for nine major rain events during the period when the disdrometers were separated by 0.65, 1.05, and 1.70 km.

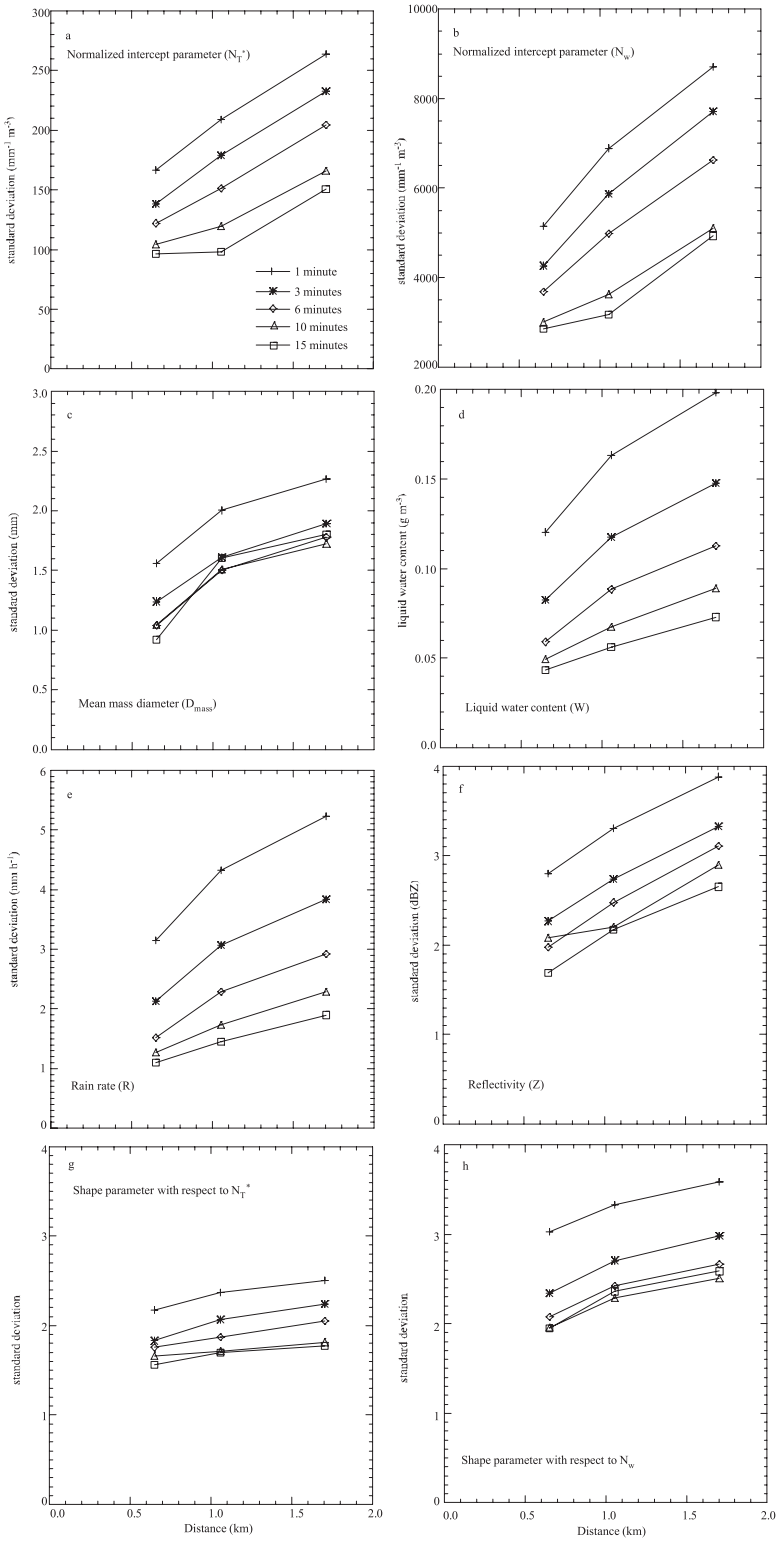

FIG. 6. The standard deviation of (a) normalized intercept parameter N_T^*, (b) normalized intercept parameter N_w, (c) mean mass diameter, (d) liquid water content, (e) rain rate, (f) reflectivity, (g) shape parameter with respect to N_T^*, and (h) shape parameter with respect to N_w for nine major rain events during the period when the disdrometers were separated by 0.65, 1.05, and 1.70 km.

and 2.0 and from 2.1 and 2.7, respectively (Figs. 6g,h). The corresponding FSD ranged from 0.36 to 0.44 and from 0.39 to 0.51. The increases in SD and FSD of the normalized DSD parameters with distance and the magnitude of these statistics were significant, demonstrating the variability of DSDs within the radar pixel space.

Among integral rain parameters, the liquid water content had a SD from 0.059 to 0.113 g m^{-3} at the shortest and longest distances, respectively (Fig. 6d), and the corresponding FSD were 0.36 and 0.69. The SD of rain rate ranged from 1.5 to 2.9 mm h^{-1} (Fig. 6e), which corresponded to FSD of 0.45 and 0.87, respectively. The SD of reflectivity, on the other hand, was between 1.9 and 3.1 dBZ (Fig. 6f) and corresponding FSD were 0.08 and 0.13. The reflectivity was the only parameter where the statistics were based on its logarithmic values. Like DSD parameters, the integral parameters showed significant increase in SD and FSD.

The correlation coefficient decreased with distance and increased with longer time averaging. Considering 6-min average statistics as a reference, the correlation of N_T^* decreased from 0.977 to 0.940 from the shortest to the longest separation distances, respectively (Fig. 7a). The correlation of N_w followed the same trend and decreased from 0.981 to 0.968 (Fig. 7b). The correlation of mean mass diameter had a steeper decrease with distance from 0.975 to 0.929 (Fig. 7c). The shape parameters in Eqs. (5) and (6) had lower correlations decreasing from 0.883 to 0.835 and from 0.838 to 0.730, respectively (Figs. 7g,h). Considering integral rain parameters, the liquid water content and rain rate had similarities as their correlations decreased from 0.984 to 0.942 and from 0.983 to 0.934, respectively (Figs. 7d,e). The correlations of reflectivity, on the other hand, had a range from 0.980 to 0.951 (Fig. 7f). With regard to rain gauge–based studies, the correlations of rainfall were higher in this study. This is partly due to the differences in rainfall characteristics as Krajewski et al. (2003) demonstrated drastic differences in correlations between the midlatitude and subtropical stations. More importantly, this is due to the differences in data retrieval between disdrometer and gauge studies. The database in this study included only those periods when all three disdrometers were reporting rainfall, while the gauge-based studies includes a network of gauges and are not inclusive of all gauges reporting. The gauge sampling errors, which will be examined in the next section, could also contribute the differences in correlations.

9. Rain gauge simulations

The gauge-based small-scale variability of rainfall studies mentioned in the introduction employed tipping-bucket gauges that suffer from severe sampling errors in light rainfall. In addition, the time stamp difference between two consecutive tips is often long enough (e.g., greater than 1 h) to consider the continuous rainfall as two different rain events. For a gauge bucket with 0.01-in. (0.254 mm) resolution, a continuous rainfall at uniform intensity of $\leq$0.25 mm h^{-1} will take >1 h for a single tip to occur. Rain intermittence, commonly observed in light rainfall, extends the duration for a tip to occur. So, we asked a question: If this study had been done through rain gauge measurements, what would be the role of gauge sampling errors?

In this regard, 1-min disdrometer measurements were employed to simulate the rain gauge measurements. We first determined the time of gauge tips where each tip corresponds to 0.254 mm and then applied a cubic spline algorithm to the simulated gauge measurements to obtain gauge rain rates at 1-min resolution (Wang et al. 2008). The cumulative distributions of rain occurrence of disdrometric and simulated gauge measurements at 1-min resolution had a difference of 2.5 dBR at the 15th percentile, while the difference decreased to 0.5 dBR at the 80th percentile (Fig. 8a). The differences in cumulative distributions of rain amount were less than 0.5 dBR except near the 65th percentile where the discreteness of the tipping-bucket gauge measurements was evident even after cubic spline interpolation (Fig. 8a). The cubic spline resulted in a higher percent of light rain in simulated gauge measurements than in the disdrometer measurements, but this had literally no effect on the distribution of rain amount as shown in 3-, 6-, and 10-min averaged cumulative distributions (Figs. 8b–d). The time averaging shifted the distribution to lighter rainfall as expected. The minimum rainfall that was set to 0.1 mm h^{-1} through the disdrometer data processing algorithm was 0.01 mm h^{-1} in 10-min average distributions. This is of course due to the presence of only one rainy minute in a 10-min interval.

The simulated gauge rainfall measurements also showed that the differences in rainfall do not necessarily increase with distance within 2 km. Table 8 shows that about 57%–62% of the observations had greater rain rate differences between the two farthest stations than the rain rate differences between the two closest stations. In contrast, only 20%–25% of observations showed the increase in rain rate difference with distance for all three distances. With respect to the disdrometer measurements in Table 6, the simulated gauge measurements had up to 6% less rain minutes of similar statistics.

The rainfall statistics were derived from simulated gauge measurements for the periods where all three instruments were reporting rainfall. The SD of rain rate

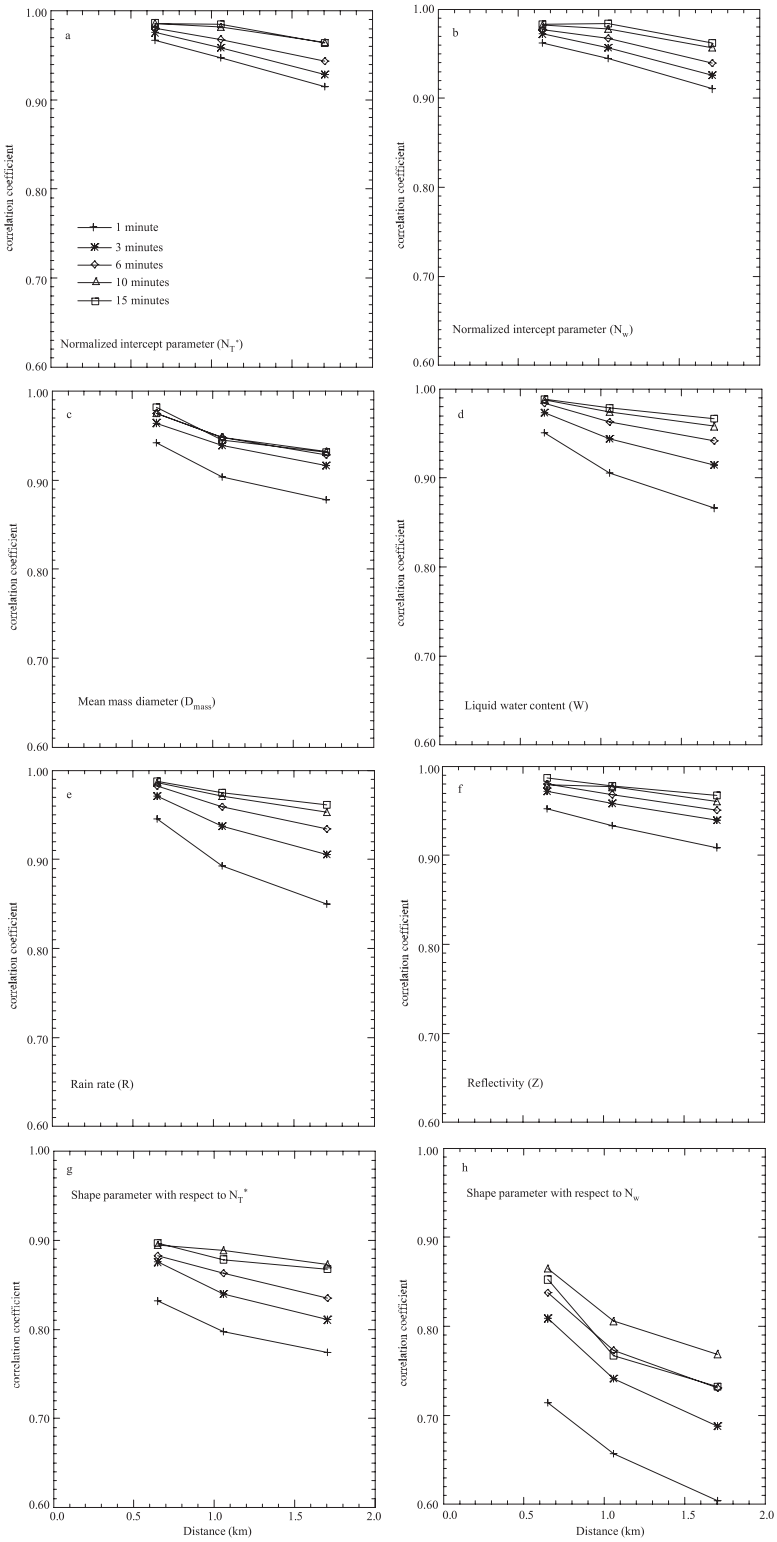

FIG. 7. As in Fig. 6, but for the correlation coefficient.

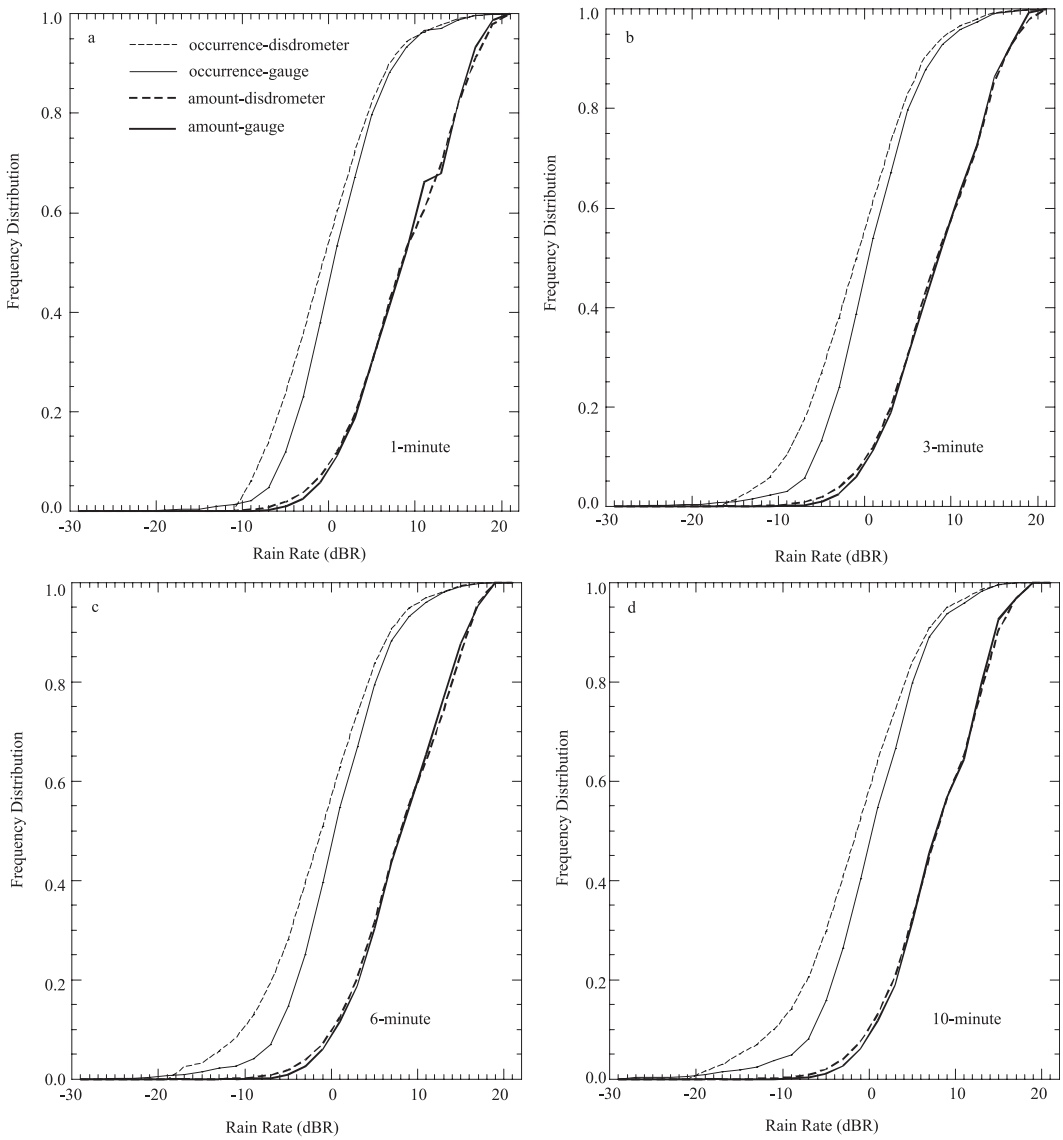

FIG. 8. Cumulative probability distribution of disdrometer and simulated gauge rain amount and rain occurrence when the disdrometer and simulated gauge measurements were averaged for (a) 1, (b) 3, (c) 6, and (d) 10 min.

based on simulated gauge measurements was higher than that based on disdrometer measurements (Fig. 9a). Considering 6-min average as a reference, the SD of rain rate based on simulated gauge was 1.9 and 3.3 mm h^{-1} at the shortest and longest separation distance, respectively. The corresponding FSD based on simulated gauge were 0.42 and 0.75 at the shortest and longest separation distance, respectively. The correlation coefficients of rain

TABLE 8. As in Table 6, but where D1, D2, and D3 represent $|\Delta G|$ (0.65 km), $|\Delta G|$ (1.05 km), and $|\Delta G|$ (1.70 km), respectively.

Time averaging (min)	D3 > D1 (%)	D3 > D2 (%)	D2 > D1 (%)	D3 > D1 and D3 > D2 (%)	D3 > D1 and D2 > D1 (%)	D3 > D2 and D2 > D1 (%)
1	57.13	51.63	54.71	37.38	39.82	20.06
3	58.93	52.72	55.15	38.79	41.22	21.08
6	59.04	53.96	56.21	39.78	41.93	22.69
10	61.57	54.47	59.26	40.89	46.14	25.46
15	62.31	55.77	57.08	43.35	43.79	24.84

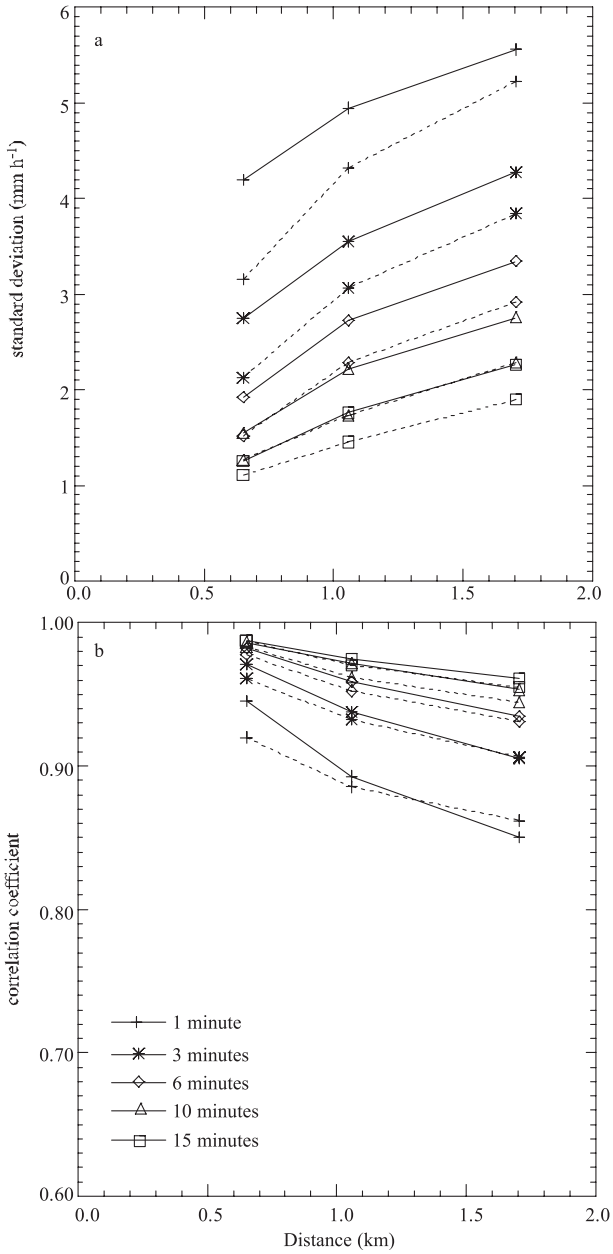

FIG. 9. The (a) standard deviation and (b) correlation coefficient of simulated gauge rain rates (solid lines) and disdrometer rain rates (dashed lines, same as in Figs. 5–8) during the period when the disdrometer were separated 0.65, 1.05, and 1.70 km and when the disdrometer measurements were averaged for 1, 3, 6, 10, and 15 min.

rate based on simulated gauge were lower than that based on disdrometer except for the 1- and 3-min averages at the longest distance (Fig. 9b). For 6-min average, the correlations based on simulated gauge ranged from 0.977 to 0.931 between the shortest and longest distance, respectively.

10. Conclusions

An experimental study of small-scale variability of DSDs has been undertaken at Wallops Island, Virginia, where three Joss–Waldvogel disdrometers were operated at distance of 0.65, 1.05, and 1.70 km in a nearly straight line for about four months. The purpose of the study was to examine the variability of DSDs and their integral parameters of liquid water content, rain rate, and reflectivity within a 2-km array, the pixel size of a typical ground-based radar. Considering polarimetric-radar-based DSD estimation, special attention was given to the variability of normalized gamma DSD parameters within a radar pixel.

The overall rain accumulations were 2.5% and 5.0% higher at the disdrometer at the southern site of the network than the disdrometers at the middle and opposite side of the network, respectively, while the disdrometer at the middle recorded more rainy minutes than both end units. The differences were attributed in part to the natural variability of rainfall and in part to the disdrometer data processing. With a few exceptions, the experiment-long composite raindrop size distributions showed good agreement. In one event, one of the disdrometers had more midsize and large drops resulting in noticeable differences in integral rainfall parameters. There were two other events where one of the units had more large drops resulting in differences in reflectivity more than 1 dBZ.

The sample size is often a point of discussion of critics when *point* disdrometer measurements are used to derive rain rainfall relations or other related applications. For the purpose of this study, the instantaneous (1 min) measurements are the most appropriate; however, the sample size is the smallest unless the rain–no-rain threshold has been raised to higher number of total drops and higher minimum rain rate. Therefore, we presented our findings at five different time averaging periods as typically done in gauge-based studies. Since time averaging reduces the total sample size, we did not require all the minutes that were averaged to be raining, resulting in more than 500 samples for the longest (15 min) average.

The nonprecipitation region within the rainy radar pixel plays a role in radar rainfall error. In this study, a single disdrometer reported just over 10% more rainy minutes than the rainy minutes when all three disdrometers report rainfall. Similarly two out of three disdrometers reported 5% more rainy minutes than when all three were reporting rainfall. These percentages were based on a 1-min average and were less for longer averaging periods.

Considering only the minutes when all three disdrometers reported rainfall, the differences in rainfall

and reflectivity did not necessarily increase with the distance. Only 26% (27%) of the data showed rainfall (reflectivity) increases with distance. These percentages were based on 15-min averages and were less for shorter averaging periods. The probability and cumulative distributions of gamma-fitted DSDs and integral rain parameters showed small variability between the three sites. This is partly due to the fact that a number of storms traveled along the track of the disdrometers. Also, in the presence of widespread stratiform rain, the differences in DSDs between the sites were less than that in relatively infrequent convective rain. At a given time, however, substantial variations were observed in gamma-fitted DSDs and integral rain parameters as shown by decrease in correlations and increase in SD and FSD. With 6-min averaging, the SD of mean mass diameter exceeds 0.11 mm at the farthest distance between the three units. The SD of rain rate, on the other hand, was near 3 mm h^{-1}, while the SD of reflectivity exceeded 3 dBZ at the longest separation distance. The correlations were above 0.9 for a gamma-fitted DSD and integral rain parameters except derived shape parameters. At the farthest separation distance and at 6-min average, the correlations were 0.939, 0.935, and 0.951 for mean mass diameter, rain rate, and reflectivity, respectively. In comparison to the gauge-based studies, the correlations were relatively high and this is attributed to the differences in data processing and precipitation climatology of region. Regarding data processing, it should be restated that the requirement of all three instruments reporting rainfall results in higher correlations and lower standard deviations.

Gauge sampling errors were also considered as one of the reasons for differences in correlations between this and gauge-based studies. The gauge rainfall was simulated using disdrometer measurements. The cumulative distributions of disdrometer and simulated gauge measurements showed substantial differences in occurrence at low percentages. For the small-scale variability, the correlations were slightly lower and SD was noticeable higher with simulated gauge measurements. It should be added that the gauge sampling errors are often observed at light rain events where the number of tips are three or less. These events were not included in this study. There was also no rain intermittence in the study.

As stated in the title, this was an experimental study. But it was also unique since the disdrometer-based small-scale variability studies are rare in the literature. Considering the design of the experiment, it is desirable to have additional disdrometers at one of the three sites to demonstrate the variability of DSDs and integral rain parameters and take these findings as a reference. Unfortunately, this was not feasible at the time this experiment. As a follow-up study, we distributed four disdrometers along the strip where the separation distances ranged from 0.4 to 5.0 km. This follow-up study intends to examine the DSD variability within the satellite (e.g., TRMM) footprint.

Acknowledgments. We thank Donat Högl of Distromet, Ltd., and his colleagues for their continuous support in calibrating the Joss–Waldvogel disdrometers and providing excellent feedback. Thanks also are given to Richard Lawrence of NASA Goddard Space Flight Center and John Gerlach of NASA Wallops Flight Facility for their leadership in ground validation efforts of the TRMM program. We also acknowledge Rafael Rincon for providing his JW disdrometer that was used in this study. Many thanks are given to Jianxin (Jerry) Wang of Science Systems Application, Inc., for running a gauge interpolation algorithm with simulated gauge measurements. Discussions with Robert Meneghini of NASA Goddard Space Flight Center, Emad Habib of the University of Louisiana—Lafayette, Mirceu Grecu of the University of Maryland, Baltimore County, and David A. Marks of Science Systems and Application, Inc., were very helpful. This study was supported by NASA's TRMM program through NNX07AF45G under Ramesh Kakar, Program Scientist.

REFERENCES

Amitai, E., D. A. Marks, D. B. Wolff, D. S. Silberstein, B. L. Fisher, and J. L. Pippitt, 2006: Evaluation of radar rainfall products: Lessons learned from the NASA TRMM validation program in Florida. *J. Atmos. Oceanic Technol.,* **23,** 1492–1505.

Arnaud, P., C. Bouvier, L. Cisneros, and R. Dominguez, 2002: Influence of rainfall spatial variability on flood prediction. *J. Hydrol.,* **260,** 216–230.

Asen, W., and C. J. Gibbins, 2002: A comparison of rain attenuation and drop size distribution measured in Chilbolton and Singapore. *Radio Sci.,* **37,** 1034, doi:10.1029/2000RS002613.

Berne, A., G. Delrieu, J. D. Creutin, and C. Obled, 2004: Temporal and spatial resolution of rainfall measurements required for urban hydrology. *J. Hydrol.,* **299,** 166–179.

Bringi, V. N., V. Chandrasekar, J. Hubbert, E. Gorgucci, W. L. Randeu, and M. Schoenhuber, 2003: Raindrop size distribution in different climate regimes from disdrometer and dual-polarized radar analysis. *J. Atmos. Sci.,* **60,** 354–365.

Ciach, G. J., and W. F. Krajewski, 2006: Analysis and modeling of spatial correlation structure in small-scale rainfall in Central Oklahoma. *Adv. Water Resour.,* **29,** 1450–1463.

Datta, S., W. L. Jones, B. Roy, and A. Tokay, 2003: Spatial variability of surface rainfall as observed from TRMM field campaign data. *J. Appl. Meteor.,* **42,** 598–610.

Gebremichael, M., and W. F. Krajewski, 2004: Assessment of the statistical characterization of small-scale rainfall variability from radar: Analysis of TRMM ground validation datasets. *J. Appl. Meteor.,* **43,** 1180–1199.

Habib, E., and W. F. Krajewski, 2002: Uncertainty analysis of the TRMM ground-validation radar-rainfall products: Application to the TEFLUN-B field campaign. *J. Appl. Meteor.,* **41,** 558–572.

——, ——, and G. J. Ciach, 2001a: Estimation of rainfall interstation correlation. *J. Hydrometeor.,* **2,** 621–629.

——, ——, and A. Kruger, 2001b: Sampling errors of tipping-bucket rain gauge measurements. *J. Hydrol. Eng.,* **6,** 159–166.

Hagen, M., and S. Yuter, 2003: Relations between radar reflectivity, liquid water content, and rainfall rate during the MAP SOP. *Quart. J. Roy. Meteor. Soc.,* **129,** 477–493.

Jameson, A. R., and A. B. Kostinski, 2001: Reconsideration of the physical and empirical origins of Z-R relations in radar meteorology. *Quart. J. Roy. Meteor. Soc.,* **127,** 517–538.

Joss, J., and A. Waldvogel, 1967: Ein spectrograph für Niederschlasgstropfen mit automatischer Auswertung (A spectrograph for the automatic analysis of raindrops). *Pure Appl. Geophys.,* **69,** 240–246.

Kozu, T., and T. Iguchi, 1999: Nonuniform beamfilling correction for spaceborne radar rainfall measurements: Implications from TOGA COARE radar data analysis. *J. Atmos. Oceanic Technol.,* **16,** 1722–1735.

Krajewski, W. F., G. J. Ciach, and E. Habib, 2003: An analysis of small-scale rainfall variability in different climatic regimes. *Hydrol. Sci. J.,* **48,** 151–162.

Lee, C. K., G. W. Lee, I. Zawadzki, and K. E. Kim, 2009: A preliminary analysis of spatial variability of raindrop size distributions during stratiform rain events. *J. Appl. Meteor. Climatol.,* **48,** 270–283.

Löffler-Mang, M., and J. Joss, 2000: An optical disdrometer for measuring size and velocity of hydrometeors. *J. Atmos. Oceanic Technol.,* **17,** 130–139.

Meneghini, R., and L. Liao, 2007: On the equivalence of dual-wavelength and dual-polarization equations for estimation of the raindrop size distribution. *J. Atmos. Oceanic Technol.,* **24,** 806–820.

Miriovsky, B. J., and Coauthors, 2004: An experimental study of small-scale variability of radar reflectivity using disdrometer observations. *J. Appl. Meteor.,* **43,** 106–118.

Smith, P. L., Z. Liu, and J. Joss, 1993: A study of sampling-variability effects in raindrop size observations. *J. Appl. Meteor.,* **32,** 1259–1269.

Steiner, M., and J. A. Smith, 2000: Reflectivity, rain rate, and kinetic energy flux relationships based on raindrop spectra. *J. Appl. Meteor.,* **39,** 1923–1940.

——, and ——, 2004: Scale dependence of radar-rainfall rates—An assessment based on raindrop spectra. *J. Hydrometeor.,* **5,** 1171–1180.

Tokay, A., D. B. Wolff, K. R. Wolff, and P. Bashor, 2003: Rain gauge and disdrometer measurements during the Keys Area Microphysics Project (KAMP). *J. Atmos. Oceanic Technol.,* **20,** 1460–1477.

——, P. G. Bashor, and K. R. Wolff, 2005: Error characteristics of rainfall measurements by collocated Joss–Waldvogel disdrometers. *J. Atmos. Oceanic Technol.,* **22,** 513–527.

van Dijk, A. I. J. M., L. A. Bruijzeel, and C. J. Rosewell, 2002: Rainfall intensity–kinetic energy relationship: A critical literature appraisal. *J. Hydrol.,* **261,** 1–23.

Villarini, G., P. V. Mandapaka, W. F. Krajewski, and R. J. Moore, 2008: Rainfall and sampling uncertainties: A rain gauge perspective. *J. Geophys. Res.,* **113,** doi:10.1029/2007JD009214.

Wang, J., B. L. Fisher, and D. B. Wolff, 2008: Estimating rain rates from tipping-bucket rain gauge measurements. *J. Atmos. Oceanic Technol.,* **25,** 43–56.

Wilks, D. S., 1995: *Statistical Methods in the Atmospheric Sciences*. Academic Press, 467 pp.

Wolff, D. B., D. A. Marks, E. Amitai, B. L. Fisher, D. S. Silberstein, A. Tokay, J. Wang, and J. L. Pippitt, 2005: Ground validation for the Tropical Rainfall Measuring Mission (TRMM). *J. Atmos. Oceanic Technol.,* **22,** 365–380.

Zhang, G., J. Vivekanandan, and E. Brandes, 2001: A method for estimating rain rate and drop size distribution from polarimetric radar measurements. *IEEE Trans. Geosci. Remote Sens.,* **39,** 830–841.

Zhang, L., D. Lu, S. Duan, and J. Liu, 2004: Small-scale nonuniformity and its effects on evaluation of nonuniform beamfilling error for spaceborne radar rain measurement. *J. Atmos. Oceanic Technol.,* **21,** 1190–1197.